

# Constrained Control for Autonomous Spacecraft Rendezvous: Learning-Based Time Shift Governor

Taehyeun Kim<sup>\*,†</sup>, Robin Inho Kee<sup>†,‡</sup>, Ilya Kolmanovsky<sup>‡</sup>, and Anouck Girard<sup>§</sup>

*Department of Aerospace Engineering, University of Michigan, Ann Arbor, 48109 MI, USA*

This paper develops a Time Shift Governor (TSG)-based control scheme to enforce constraints during rendezvous and docking (RD) missions in the setting of the Two-Body problem. As an add-on scheme to the nominal closed-loop system, the TSG generates a time-shifted Chief spacecraft trajectory as a target reference for the Deputy spacecraft. This modification of the commanded reference trajectory ensures that constraints are enforced while the time shift is reduced to zero to effect the rendezvous. Our approach to TSG implementation integrates an LSTM neural network which approximates the time shift parameter as a function of a sequence of past Deputy and Chief spacecraft states. This LSTM neural network is trained offline from simulation data. We report simulation results for RD missions in the Low Earth Orbit (LEO) and on the Molniya orbit to demonstrate the effectiveness of the proposed control scheme. The proposed scheme reduces the time to compute the time shift parameter in most of the scenarios and successfully completes rendezvous missions.

## I. Introduction

Spacecraft proximity operations (SPO) involve two spacecraft maneuvering near each other in space, e.g., to perform rendezvous and docking (RD). The primary spacecraft (referred to as the Chief) maintains a nominal orbit passively or actively, while the other spacecraft (referred to as the Deputy) is actively controlled to perform the RD mission [1] while satisfying constraints on thrust magnitude, on the line of sight (LoS) constraint of the docking port and on relative velocity.

Many spacecraft RD missions were conducted near and beyond the Earth. The first spacecraft docking mission was a part of the Gemini 8 mission, in which astronauts manually performed the docking with the target vehicle. The following RD missions were also conducted, as was done for the Apollo mission in 1969 and the Skylab mission in 1973. As docking techniques were cultivated through former missions, docking missions became complicated and required an autonomous system to ensure safety and reduce costs. The first autonomous spacecraft docking mission was performed as a part of the Orbital Express mission in 2007. As examples in private sectors, Northrop Grumman then began to provide commercial resupply services to the ISS in 2014, and SpaceX launched spacecraft docking missions for supply service to NASA and for Axiom Space in 2020. Thus, the RD techniques played a crucial role in space missions while satisfying the growing interest of the space community in complicated missions.

Various control approaches for RD have been studied. In particular, the artificial potential function (APF) methods have been applied to ensure safety to address in RD operations [2, 3]. However, the use of APFs to handle multiple constraints and simultaneous state and control constraints can be not straightforward. Model Predictive Control (MPC) based on the Clohessy-Wiltshire-Hill (CWH) linearized relative motion model has

---

<sup>\*</sup>Ph.D. candidate, Aerospace Engineering, 1320 Beal Ave, Ann Arbor, MI 48109

<sup>†</sup>Master's student, Department of Mechanical Engineering, University of Michigan

<sup>‡</sup>Professor, Aerospace Engineering, 3038 FXB, 1320 Beal Ave, Ann Arbor, MI 48109, AIAA Associate Fellow.

<sup>§</sup>Professor, Robotics and Aerospace Engineering, 3264 FMCRB, 2505 Hayward Street, Ann Arbor, MI 48109, AIAA Associate Fellow.

<sup>1</sup>These authors contributed equally to this work

been considered in [4]. However, the utilization of MPC requires addressing the computational challenges inherent in solving a discrete-time optimal control problem online. The integration of genetic algorithms (GA) with fuzzy logic controllers (FLC) has been studied in [5]. However, this approach requires a subjective selection of fuzzy membership functions and lacks formal constraint enforcement guarantees.

The use of machine learning for spacecraft control has been of growing interest [6]. Deep reinforcement learning (DRL), in particular, has been considered for autonomous guidance and proximity operation [7–11]. Guaranteeing stability and convergence with DRL can, however, be challenging [12, 13].

The Time Shift Governor (TSG) has been considered in [14–17] to enforce constraints by time shifting the target trajectory of the Chief spacecraft and adjusting the time shift to achieve safe RD. The TSG, which is a variant of the parameter governor, is an add-on scheme used for managing constraints without redesigning the closed-loop system. It has been developed for scenarios involving circular Earth orbits in the Two-Body problem setting and more complex scenarios like halo orbits in the Circular Restricted Three-Body Problem (CR3BP) setting [14, 16]. Unlike general nonlinear model predictive controllers that solve high-dimensional optimization problems, TSG reduces the optimization problem to optimizing a single time shift parameter.

In this paper, we consider an imitation learning motivated approach to the implementation of TSG which involves the use of a Long Short Term Memory (LSTM) network [18, 19] to approximate the optimal time shift. The neural network is trained using data from offline simulation of the closed-loop system with TSG and then deployed for the onboard use to compute the time shift parameter without requiring iterative optimization. Notably, we find that by using a sequence of past states as the input to LSTM we are able to improve approximation accuracy with LSTM as compared to only using the current state. We also propose a hybrid variant of the algorithm where the TSG online optimization involving bisections is only performed if the time shift parameter generated by the LSTM neural network is not safe due to approximation errors.

This paper is organized as follows: In Section II, we summarize the coordinate systems, spacecraft translational dynamics model, the nominal controller, as well as the constraints considered during the RD mission. Then, in Section III, we introduce the TSG to enforce the constraints. Section IV introduces our Learning-based TSG (L-TSG), which integrates an LSTM network with a phase-adaptive sliding window and a custom loss function, further enhanced by a hybrid prediction algorithm. Section V reports the numerical results, demonstrating the efficacy of our approach. Finally, Section VI concludes the paper with a summary of contributions and potential directions for further research.

## II. Problem Formulation

In our study, we consider a docking mission involving the Deputy and the Chief spacecraft on orbit, with mission-specific constraints. This section will detail the coordinate systems, dynamic models, control strategies, and constraints that define our approach to the RD mission. We assign the subscripts  $c$  and  $d$  to denote the Chief and Deputy spacecraft respectively, while the subscript  $i$  is used to denote a spacecraft that could be either the Chief or the Deputy.

### A. Coordinate systems

In this work, two right-handed coordinate systems are employed to describe the spacecraft equations of motion and relative motion, as shown in Fig . 1. The origin of the Earth-centered inertial (ECI) frame,  $\mathcal{E} : \{\hat{x}_{\mathcal{E}}, \hat{y}_{\mathcal{E}}, \hat{z}_{\mathcal{E}}\}$ , is at the center of the Earth  $O_{\mathcal{E}}$ , with the  $\hat{x}$ -axis pointing towards the vernal equinox—the direction from the Earth to the Sun at noon on the day of the spring equinox, the  $\hat{z}$ -axis pointing towards the Earth’s rotational axis, and the  $\hat{y}$ -axis completing the right-handed system.

The local Velocity-Normal-Binormal (VNB) frame,  $\mathcal{L} : \{O_c, \hat{x}_{\mathcal{L}}, \hat{y}_{\mathcal{L}}, \hat{z}_{\mathcal{L}}\}$ , is also defined to describe the relative motion of objects with respect to the Chief spacecraft. Unlike the ECI frame, the VNB frame is a rotating and accelerating coordinate system and has its origin at the center of mass of the Chief spacecraft  $O_c$ .

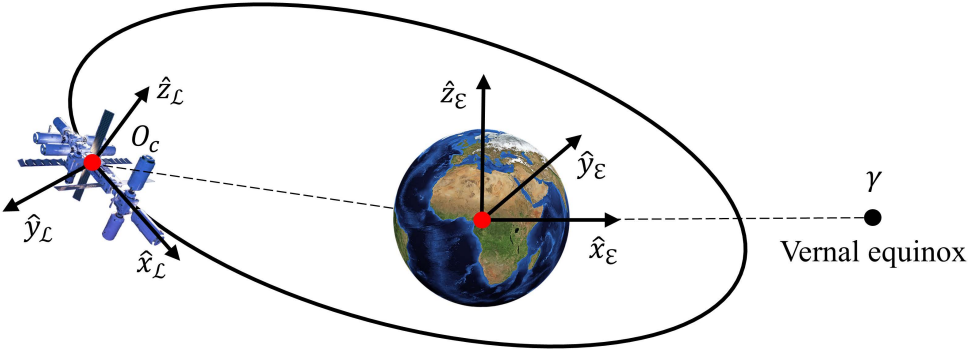


Fig. 1 ECI and VNB coordinate systems.

with three orthonormal vectors which are defined as

$$\hat{x}_\mathcal{L} = \frac{v(X_c)}{\|v(X_c)\|}, \quad \hat{y}_\mathcal{L} = \frac{p(X_c) \times \hat{x}_\mathcal{L}}{\|p(X_c) \times \hat{x}_\mathcal{L}\|}, \quad \hat{z}_\mathcal{L} = \hat{x}_\mathcal{L} \times \hat{y}_\mathcal{L}, \quad (1)$$

where  $p(\cdot), v(\cdot) : \mathbb{R}^6 \rightarrow \mathbb{R}^3$  are functions that map from a state to position and velocity, respectively, expressed in the ECI frame.

## B. Dynamics

The equations of motion of spacecraft are given by

$$\dot{X}_i = f(t, X_i(t), u_i(t)), \quad (2)$$

where  $X_i = [x_i, y_i, z_i, \dot{x}_i, \dot{y}_i, \dot{z}_i]^\top$ , for  $i \in \{c, d\}$ , and  $u_i = [u_{1,i}, u_{2,i}, u_{3,i}]^\top$  denote the spacecraft state and the control input to the spacecraft, expressed in the ECI frame. Note that the Chief spacecraft maintains its nominal orbit without using control input, i.e.,  $u_c = 0$ , while the Deputy spacecraft uses control input to track the target. In this work, we omit the subscript  $d$  in the control input, i.e.,  $u = u_d$ . The translational equations of motion for spacecraft are given as,

$$\ddot{\vec{r}}_i = -\frac{\mu}{r_i^3} \vec{r}_i + \vec{u}_i, \quad (3)$$

where  $\mu$  stands for the gravitational parameter,  $\vec{r}_i$  is the spacecraft position vector and  $r = \|\vec{r}\|$  is its 2-norm.

## C. Discrete Time Linear Quadratic Controller

Since the TSG is an add-on scheme, we need a nominal controller that is (locally) stabilizing to a target along the reference orbit. In this work, the discrete-time linear quadratic (DTLQ) controller is implemented to provide an optimal control solution stabilizing the Deputy spacecraft to the target.

While the Chief spacecraft is assumed to follow a reference orbit, which is an unforced natural motion, the Deputy spacecraft motion is controlled by the feedback controller

$$u_d(t) = K(t_k)(X_d(t_k) - X_v(t_k)), \quad t_k \leq t < t_{k+1}, \quad (4)$$

where  $X_v(t)$  is the virtual target, which is determined by the TSG, and  $K$  is the periodic LQR gain which is calculated for the linearization of (2) along the state trajectory on the reference orbit. To save computational effort, the standard infinite-horizon LQ control gain  $K$  is pre-computed for an orbit as

$$K(t_k) = (B_d^\top S B_d + R)^{-1} B_d^\top S A_d, \quad (5)$$

where  $S$  is the infinite horizon solution of the Discrete Algebraic Riccati Equation (DARE),

$$S = Q - A_d^\top(t_k) S B_d (R + B_d^\top(t_k) S B_d(t_k))^{-1} B_d^\top(t_k) S A_d(t_k) + A_d^\top(t_k) S A_d(t_k), \quad (6)$$

where  $Q \succeq 0$  and  $R > 0$  are the weighting matrices associated with the state and control, respectively, and  $S$  stands for the solution of DARE at the time instant  $t_k$ , e.g.,  $S = S(t_k)$ . Here  $A_d(t_k)$  and  $B_d(t_k)$  represent the discrete-time linearized model at the virtual target state. Note that we assume that the nominal controller, i.e., the DTLQ controller, is able to track a virtual target  $X_v(t)$ , which is a time-shifted state trajectory of the reference orbit.

#### D. Constraints

In this paper, we consider the state and control input constraints for the Deputy spacecraft. During the RD mission, the Deputy spacecraft is maintained within the safe approach corridor from the docking port, assuming that the docking port is towards the opposite direction of the Chief spacecraft's velocity direction. This ensures that the docking port of the Deputy spacecraft and the Chief spacecraft is aligned. The Line of Sight (LoS) constraint is written as

$$h_1 = -\frac{v(X_c)^\top p(X_d - X_c)}{\|v(X_c)\| \|p(X_d - X_c)\|} + \cos(\alpha) \leq 0, \quad (7)$$

where  $\alpha$  is a LoS half-cone angle.

The physical limit of the thrust magnitude is expressed as

$$h_2 = \|u_d\| - u_{\max} \leq 0, \quad (8)$$

where  $u_{\max}$  is the maximum total magnitude of the physical thrusters. Considering that the spacecraft typically uses a single main thruster for maneuvers, we assume that the attitude control system accurately aligns the spacecraft consistently with the desired thrust direction. To achieve faster response, we enforce the constraint in Eq. (8) using a saturation function rather than addressing Eq. (8) as a constraint by the TSG. The control input, limited by the saturation, is determined as

$$u_d(t) := \min(\|u_d(t)\|, u_{\max}) \cdot \hat{u}_d(t), \quad (9)$$

where  $\hat{u}_d(t) = u_d(t)/\|u_d(t)\|$ . Note that the prediction of the closed-loop response in the TSG accounts for the saturated control in Eq. (9) to enforce Eq. (8).

We limit the relative velocity magnitude of the Deputy spacecraft with respect to the Chief spacecraft to avoid the risk of high relative velocity collisions. Hence, the soft docking constraint is defined as

$$h_3 = \|v(X_d - X_c)\| - \gamma_2 \|p(X_d - X_c)\| - \gamma_3 \leq 0, \text{ if } \|p(X_d - X_c)\| \leq \gamma_1, \quad (10)$$

where  $\gamma_1$ ,  $\gamma_2$  and  $\gamma_3$  are predetermined mission specific parameters.

### III. Time Shift Governor

As a variant of the parameter governor [20], the Time Shift Governor (TSG) is an add-on scheme that enforces state and control constraints, see in Fig. 2. In this paper, we apply TSG to the spacecraft rendezvous and docking (RD) problem. TSG generates a virtual target trajectory, which is determined as time-shifted trajectory of the Chief spacecraft, by solving a one dimensional constrained optimization problem.

More specifically, assuming that the Deputy spacecraft is behind the Chief spacecraft in orbital track, to satisfy the constraints, the TSG computes the smallest in magnitude non-positive time shift, which represents

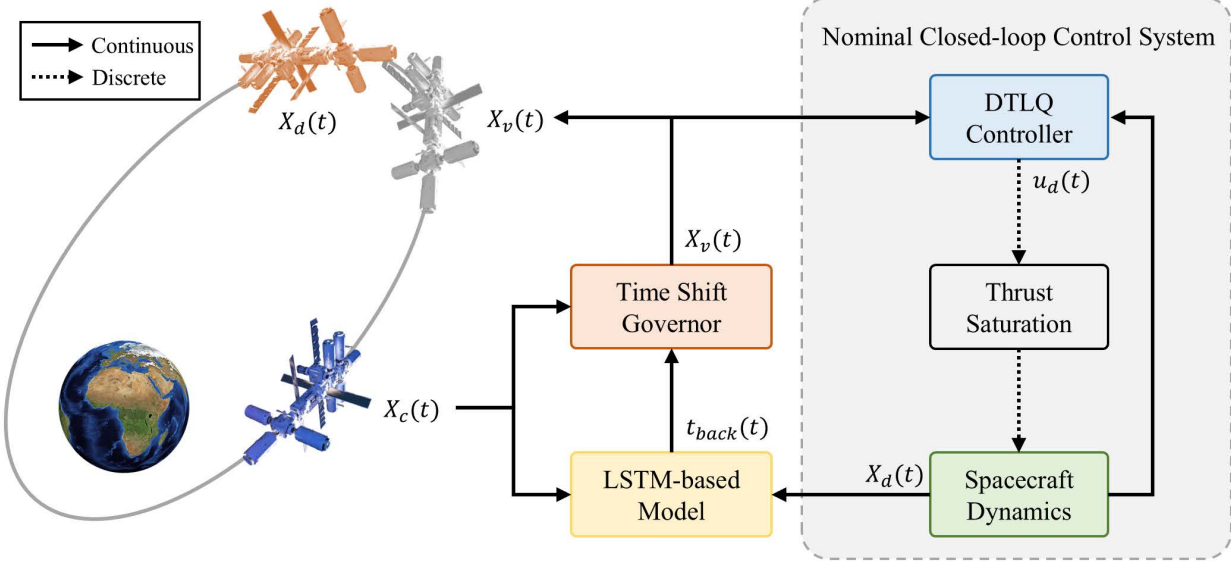


Fig. 2 Diagram of the control system architecture incorporating learning-based predictive model with TSG and DTLQ controller.

the minimum difference in time between a virtual target and the Chief spacecraft along the orbital track, and such that the predicted trajectory assuming the time shift is maintained constant at that value is guaranteed to satisfy the constraints. The TSG then provides the virtual target corresponding to this time shift, i.e.,

$$X_v(t) = X_c(t + t_{\text{back}}(t)), \quad (11)$$

where  $t_{\text{back}}(t) = t_{\text{back}}(t_k)$  for  $t \in [t_k, t_{k+1})$  is the time shift, which is thus a piecewise constant function of time. Additionally, the LQ control gain  $K$  is precomputed for one orbit period and implemented using linear interpolation.

For TSG to be able to successfully enforce the constraints, at the initial time instant, there must exist a feasible time shift that guarantees that the predicted trajectory corresponding to that time shift will satisfy constraints over a sufficiently long horizon. For TSG to be able to gradually converge the time shift to zero (i.e., for Deputy spacecraft to actually be able to reach the Chief spacecraft), TSG must be able to make at least small adjustments in the time shift when the Deputy spacecraft state is sufficiently close to the state on the target orbit corresponding to the constant value of the time shift without causing constraint violations by the predicted trajectory.

In the implementation of TSG in this paper, we use the prediction horizon of one orbital period of the Chief spacecraft to check whether the constraints are satisfied. The initial time shift parameter is determined by finding the state along the nominal trajectory of the Chief spacecraft closest to the state of the Deputy spacecraft. At the subsequent time instants, bisections are used to solve the one dimensional optimization problem and compute the time shift where the search interval is restricted to the one between the previous time shift (feasible by construction) and zero.

#### IV. Learning-based Time Shift Governor (L-TSG)

In this section, we introduce a novel framework that accelerates the Time Shift Governor (TSG) onboard computations through the use of a deep-learning model to approximate the solution of the TSG optimization problem thereby providing an explicit or an imitation learning based solution. This deep learning model utilizes a Long short-term memory (LSTM) layer and a fully connected layer to map sequential data input into

the time shift parameter. The proposed L-TSG computes the time shift parameter which results in enforcing constraints and accomplishing the rendezvous mission. We apply a phase-adaptive sliding window (PA-SW) approach to enhance the performance of the deep learning model during the RD mission. It is important to note that, in an ideal case, the deep learning prediction model can generate the time shift parameter just as a function of the combined state of the Deputy and Chief spacecraft at a given time instant. However, the deep learning model may be able to compute a more accurate approximation of the optimal time shift from a sequence of past state instead of only the current state as it may be able to more easily evolve necessary representation during training. In the training process, we utilize a loss function based on a problem-specific heuristic.

The time shift prediction from the LSTM model has an approximation error, which is a potential reason for causing constraint violations. L-TSG first checks constraint violation over the prediction horizon and then determines whether it updates the time shift. If the time shift prediction is valid, the L-TSG uses the time shift while, if not, applying the conventional TSG with a set of time shifts, i.e.,  $\mathbb{R}_{[t_{\text{back}}^-, 0]}$ , which is bounded by the previous time shift parameter  $t_{\text{back}}^-$  and zero. With this framework, L-TSG reduces an average computation time and bounds the worst-case computation time to that of the conventional TSG.

## A. Data Preparation

The dataset consists of 500 trajectories corresponding to different initial states of the Deputy spacecraft,  $X_d(t_0)$ , and with the conventional TSG based on bisections implemented to enforce the constraints. We allocate the dataset as follows: 60% for training, 20% for validation, and 20% for testing. To enhance the training performance, we use Min-Max normalization to scale the time shift values to a range between zero and one, i.e.,  $t_{\text{back}}^{(\min/\max)} \in [0, 1]$ , maintaining the original distribution of the data without distortion of information. This facilitates faster convergence of the neural network training.

## B. Network Architecture

In this study, we use the LSTM network with the input, output, and forget gates in Fig. 3 for the time shift parameter prediction model. LSTMs are often used to capture temporal dependencies in sequential data by maintaining a memory of previous states through their gating mechanism [18, 19]. The cell state updates utilize the Hadamard product,  $\odot$ , allowing for element-wise multiplication of the input, forget, and cell gates. The proposed LSTM network maps a sequence of the Chief and Deputy spacecraft's states to the time shift parameter.

The use of sequential data allows LSTM network to account for temporal dependencies, that could be important for accurate predictions. The LSTM cell encodes the sequential information of the spacecraft states, encapsulating the resulting trajectory and imposed constraints. The fully connected neural network then decodes the encoded data from the state sequence to the output of the predicted time shift. Compared to the Multilayer Perceptron (MLP), the LSTM cell can achieve better performance by capturing temporal dependencies in the sequential data [21].

The LSTM-based model is thus a mapping from the past sequence of Chief and Deputy spacecraft states to the time shift parameter:

$$t_{\text{back}} = \Gamma_{\text{Pred}}(W(t_k)), \quad (12)$$

where  $W(t_k)$  is a window of sequential data at time step  $t_k$ .

Fig. 4 illustrates the network architecture, implemented using PyTorch. To enhance stability and efficiency in training, we first apply a batch normalization layer to standardize inputs. An LSTM layer then processes the sequential data in a specified window. To address the overfitting problem, we use the dropout layer to randomly disable a portion of the inputs. Then, a fully connected layer translates the hidden states of the LSTMs as inputs for the sigmoid function. The sigmoid function constrains the output values between 0

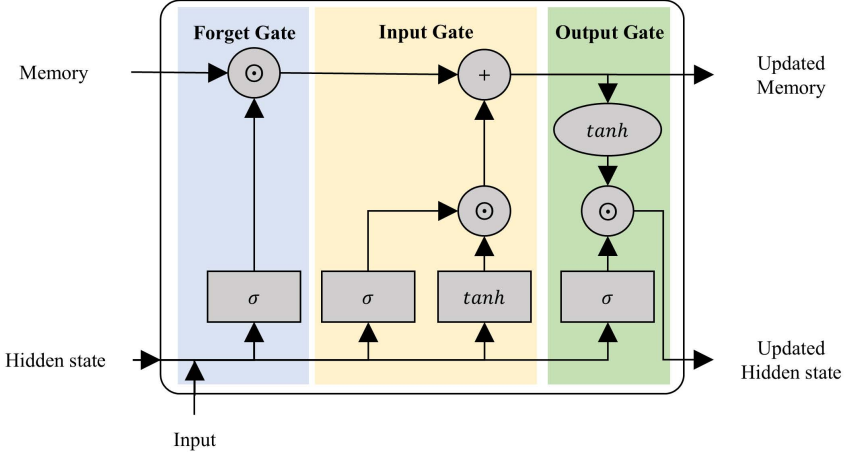


Fig. 3 Diagram of the LSTM cell, illustrating the input, forget, and output gates.

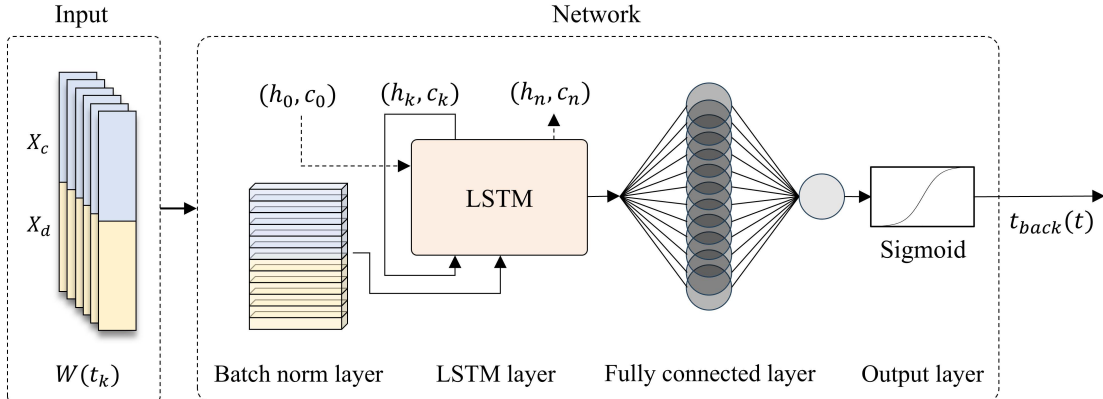


Fig. 4 Overview of LSTM-based time shift prediction model network architecture.

and 1, aligning with the range established by the Min-Max scaling method applied during data preparation, ensuring consistency in the network's predictions.

### C. Phase-Adaptive Sliding Window (PA-SW) Approach

We implement a PA-SW approach to enhance the efficiency and accuracy of our prediction model during the RD mission. This approach involves dynamically adjusting the window size based on the current phase of the mission, defined by the relative distance between the Deputy and Chief spacecraft. Sliding window approaches have been previously used to handle sequential data [22, 23], and we modify this approach to implement an effective prediction model corresponding to the specific phases of the RD mission. By adapting the window size according to the mission phase, our approach ensures efficient data utilization and computational cost reduction throughout the mission.

For the Crew-3 mission, which includes two phases (distances over 1km, and 1km to 0km), three models are used distinguished by window sizes: window size of  $w_k = 1$  for the initial time,  $w_k = 2$  for the first phase (over 1km), and  $w_k = 3$  for the second phase (1km to 0km). This ensures that as the spacecraft gets closer, the window size increases, enhancing prediction accuracy during the critical close-range phase. For the Molniya orbit mission, which also consists of two phases (distances over 1km, and 1km to 0km), two models are used,

both with the same window size of  $w_k = 100$ . Since a larger window size is already in place, it remains consistent for both phases, ensuring accuracy without requiring further adjustment. The window is adjusted as:

$$W(t_k) = \{[X_c^\top(t_j), X_d^\top(t_j)]^\top \in \mathbb{R}^{12 \times w_k} \mid j \in \mathcal{I}_w(t_k)\}, \quad (13)$$

where  $\mathcal{I}_w(t_k) = \{j \in \mathbb{N} \mid j = \max(0, k - w_k + 1), \dots, k\}$  is a set of indices in the dynamic sliding window at time step  $k$  and  $w_k$  is the window size, which is set dynamically based on the mission phase.

This phase-adaptive strategy ensures that immediate and appropriate predictions are made with the available data, allowing the model to adapt as more data becomes available and as the Chief spacecraft is approached where the constraints become more prominent.

#### D. Custom Loss Function

We design a loss function that incorporates the mean squared error (MSE) and a heuristic term penalizing predicting small in magnitude time shifts than in the data which could be unsafe. MSE minimizes the average squared discrepancy of predictions with respect to the target values. Specifically, the loss function based on the MSE alone enables a prediction model to generate smaller time shift estimates than in the data which could be unsafe and lead to constraint violation. Thus, beside the MSE in the loss function, we augment a penalty term, which is the mean squared ReLU (MSReLU), with a penalty weight  $\eta$ , i.e.,

$$\mathcal{L}_{\text{Total}} = \mathcal{L}_{\text{MSE}} + \eta \cdot \mathcal{L}_{\text{MSReLU}}, \quad (14)$$

where

$$\mathcal{L}_{\text{MSE}} = \frac{1}{N} \sum_{i=1}^N (\hat{y}_i - y_i)^2, \quad \mathcal{L}_{\text{MSReLU}} = \frac{1}{N} \sum_{i=1}^N (\text{ReLU}(\hat{y}_i - y_i))^2, \quad (15)$$

and where  $\hat{y}_i$  and  $y_i$  denote the predicted time shift and the target time shift, respectively, and  $N$  is the total number of samples. MSReLU applies penalties when prediction errors are positive, considering that the target time shift is the maximum time shift to satisfy the constraints. In the other setting with the Deputy spacecraft approaching from the positive V-bar direction, the MSReLU function becomes  $\mathcal{L}_{\text{MSReLU}} = \frac{1}{N} \sum_{i=1}^N (\text{ReLU}(y_i - \hat{y}_i))^2$ . Note that the use of the square in MSReLU term enhances differentiability and improves unit matching with the MSE term.

#### E. Hyperparameter Tuning

In optimizing hyperparameters for the LSTM-based prediction model, we use the grid search algorithm to find the optimal hyperparameter combination within the accessible hyperparameter space. The hyperparameters are defined as follows: A hidden state space  $\{h \in \mathbb{N} \mid 2^s, s = 6, 7, 8\}$ , dropout rate  $\delta \in \{0.1, 0.15, \dots, 0.3\}$ , batch size space  $\{N \in \mathbb{N} \mid 2^s, s = 7, 8, 9, 10, 11\}$ , learning rate space  $\{\lambda \in \mathbb{R} \mid s_1 \times 10^{s_2}, s_1 = 5, 2, 1, s_2 = -3, -4, -5\}$ , and the penalty weight  $\eta \in \{0.1, 0.5, 1.0, 10, 100\}$  in Eq. (14). We utilize a maximum of 300 epochs and apply an early stopping mechanism with a patience parameter of 15 epochs to save training time and prevent overfitting.

Moreover, to enhance the robustness and generalizability of our model, we incorporate a 10-fold cross-validation process. This method splits the dataset into 10 subsets, using each part once as the validation set while the remaining 9 parts are used as a training set. The optimal hyperparameters for each window size were those that minimized the mean validation loss of the cross-validation process, which was set to be the same custom loss function used during training. This consistency in loss functions across training and validation stages ensures that the performance metrics are directly comparable, enhancing the reliability of our model evaluation.

## F. Hybrid TSG Algorithm

We combine a learning-based model with a TSG that uses the bisection algorithm. The learning-based model computes the time shift as a function of the states which is then verified through forward simulations; if the verification fails, the algorithm reverts to the bisection-based TSG. This approach reduces the computing time of the time shift parameter in most of the cases. More specifically, our proposed hybrid algorithm computes a time shift  $t_{\text{back}}$  based on  $W(t_k)$  as follows:

- 1) **Time Shift Estimation:** Every update period  $P_{\text{TSG}}$ , our learning-based model estimates the time shift  $t_{\text{back}}$  corresponding to  $W(t_k)$ , e.g.,  $t_{\text{back}} = \Gamma_{\text{Pred}}(W(t_k))$ .
- 2) **Virtual Target State Computation:** The state of the virtual target,  $X_v(X_c(t), t_{\text{back}})$ , is updated to the state of the Chief spacecraft corresponding to the estimated time shift in Eq. (11).
- 3) **Estimated Time Shift Verification:** We check constraint satisfaction over the predicted trajectories of the Deputy and Chief spacecraft, for a sufficiently long prediction horizon  $T_{\text{TSG}}$ , with the virtual target corresponding to the time shift estimated by the learning-based model, based on Eqs. (2) and (4). If the estimated time shift parameter is verified, the virtual target is updated corresponding to the time shift; otherwise, the previous virtual target holds.
- 4) **Verification Failure Handling:** Conventional TSG based on bisections is applied to determine the time shift.

These steps are summarized in Algorithm 1. We use  $\epsilon = 1 \times 10^{-10}$  in the implementation.

### Algorithm 1 Hybrid TSG Algorithm

```

Input:  $t_n, W(t_n), t_{\text{back}}(t_{n-1})$ 
Output:  $t_{\text{back}}(t_n)$ 
 $k_1, k_2 = 0, 0;$ 
for  $k$  in  $\{1, 2, 3, \dots, N_{\text{sim}}\}$  do
    Estimate a time shift parameter using the learning-based model:  $t_{\text{back}} = \Gamma_{\text{Pred}}(W(t_k));$ 
     $1_{\text{safe}} = \text{Verification}(t_k, X_c, X_d, t_{\text{back}}, T_{\text{TSG}});$ 
    if  $1_{\text{safe}}$  then
        if  $|t_{\text{back}}(t_k) - t_{\text{back}}(t_{k-1})| < \epsilon$  then
             $k_1 = k_1 + 1;$ 
            if  $k_1 < N_1$  then
                Use  $t_{\text{back}}(t_k)$  computed from the learning-based model.
            else
                Perform bisection search with bounds:  $t_{\text{back}} \in [t_{\text{back}}(t_{k-1}), 0]$ 
                 $k_1 = 0;$ 
            end if
        end if
    else if  $1_{\text{safe}} = \text{False}$  then
        if  $k_2 < N_2$  then
             $t_{\text{back}}(t_k) = t_{\text{back}}(t_{k-1});$ 
             $k_2 = k_2 + 1;$ 
        else
            Perform bisection search with bounds:  $t_{\text{back}} \in [t_{\text{back}}(t_{k-1}), 0]$ 
             $k_2 = 0;$ 
        end if
    end if
end if
end for

```

## V. Simulation Results

In this paper, we demonstrate the learning-based TSG (L-TSG) for spacecraft rendezvous and docking missions in circular and elliptic orbits which correspond to: Low Earth Orbit (LEO) used in the Crew-3 mission and the Molniya orbit.

### A. Simulation Specifications

In this simulation, we consider the application of our learning-based TSG (L-TSG) to Crew-3 RD mission and highly elliptic orbit, the Molniya orbit. We consider the Chief spacecraft following the reference orbit, where the orbital elements are specified in Tables 1 and 2. The LEO and Molniya orbit have a period of 92.97 minutes and 721.48 minutes, respectively. The one orbital period  $P_{\text{ref}}$  is chosen as the prediction horizon for the TSG at a time instant  $\tau$ , i.e., the prediction is performed over the time interval,  $[\tau, \tau + P_{\text{ref}}]$ . The gravitational parameter is  $\mu = 398600.4418 \text{ km}^3/\text{sec}^2$ .

The nominal controller of the Deputy spacecraft is the DTLQ controller in Eq. (4) with an LQR gain  $K(t_k)$  computed for the following state and control weighting matrices,  $Q = \text{diag}(10, 10, 10, 1, 1, 1)$ ,  $R = \text{diag}(1, 1, 1)$ . Since LTSG locates the virtual target state along the reference trajectories, the LQR gain is precomputed over one orbital period before simulations begin. Using linear interpolation, the nominal controller applies the precomputed LQR gain, which is a piecewise constant as a function of time.

In our simulations, the learning-based TSG manages the constraints specified in Eqs. (7), (8), and (10) with parameters as follows: The half-cone angle  $\alpha$  is set to  $20^\circ$ , the thrust magnitude limit  $u_{\max}$  to  $0.5 \text{ m} \cdot \text{s}^{-2}$ , and the approach velocity constraints are set with  $\gamma_1 = 5 \text{ km}$  for distance,  $\gamma_2 = 20 \text{ rad} \cdot \text{s}^{-1}$  for angular rate, and  $\gamma_3 = 0.001 \text{ km} \cdot \text{s}^{-1}$  for relative velocity limit. The Crew Dragon spacecraft, which we utilize in both missions, has a launch mass of 12,519 kg [24] and is equipped with 16 Draco engines, each capable of a maximum thrust of 400N [25], resulting in an actual thrust magnitude of  $0.5112 \text{ m} \cdot \text{s}^{-2}$ . To ensure safety, we have conservatively set the thrust magnitude limit to  $0.5 \text{ m} \cdot \text{s}^{-2}$ .

To demonstrate the robustness of the L-TSG, perturbations  $\delta X$  are added to the nominal initial state of the Deputy spacecraft  $\bar{X}_d(t_0)$ , e.g.,  $X_d(t_0) = \bar{X}_d(t_0) + \delta X$ . The perturbations on position and velocity are chosen as, respectively,  $p(\delta X) \sim \mathcal{N}(0, \sigma_{\text{pos}}^2 \cdot [I]_3)$ ,  $v(\delta X) \sim \mathcal{N}(0, \sigma_{\text{vel}}^2 \cdot [I]_3)$ , where standard deviations of position  $\sigma_{\text{pos}}$  and of velocity  $\sigma_{\text{vel}}$  are set to be a tenth of the initial relative distance of the Deputy spacecraft with respect to the Chief spacecraft and a hundredth of the initial relative velocity, respectively, e.g.,  $\sigma_{\text{pos}} = (0.1) \cdot \|p(\bar{X}_d(t_0) - X_c(t_0))\|$  and  $\sigma_{\text{vel}} = (0.01) \cdot \|v(\bar{X}_d(t_0) - X_c(t_0))\|$ . From these randomly generated initial states we then only retain initial perturbed Deputy spacecraft states  $X_d(t_0)$  that are feasible, i.e., satisfy two criteria:

- The states satisfy all the imposed constraints.
- The states have an initial time shift parameter that avoids constraint violation over the predicted trajectory for the prediction horizon  $P_{\text{ref}}$ .

### B. Simulation in Low Earth Orbit

In this scenario, the Chief spacecraft orbits along the LEO of the International Space Station (ISS) and the Deputy spacecraft nominally starts about 50 km behind the Chief spacecraft in the same orbital track.

Table 3 summarizes the estimated initial conditions of the Deputy spacecraft with respect to the Chief spacecraft in the ECI frame. This simulation employs Monte Carlo methods to introduce variations, where

| SMA, $a$         | Eccentricity, $e$ | Inclination, $i$ | RAAN, $\Omega$ | Argp, $\omega$ |
|------------------|-------------------|------------------|----------------|----------------|
| 6798.281637 [km] | 0.000551          | 0.900516 [rad]   | 5.909781 [rad] | 1.872335 [rad] |

Table 1 Classical orbital elements of the reference ISS orbit.

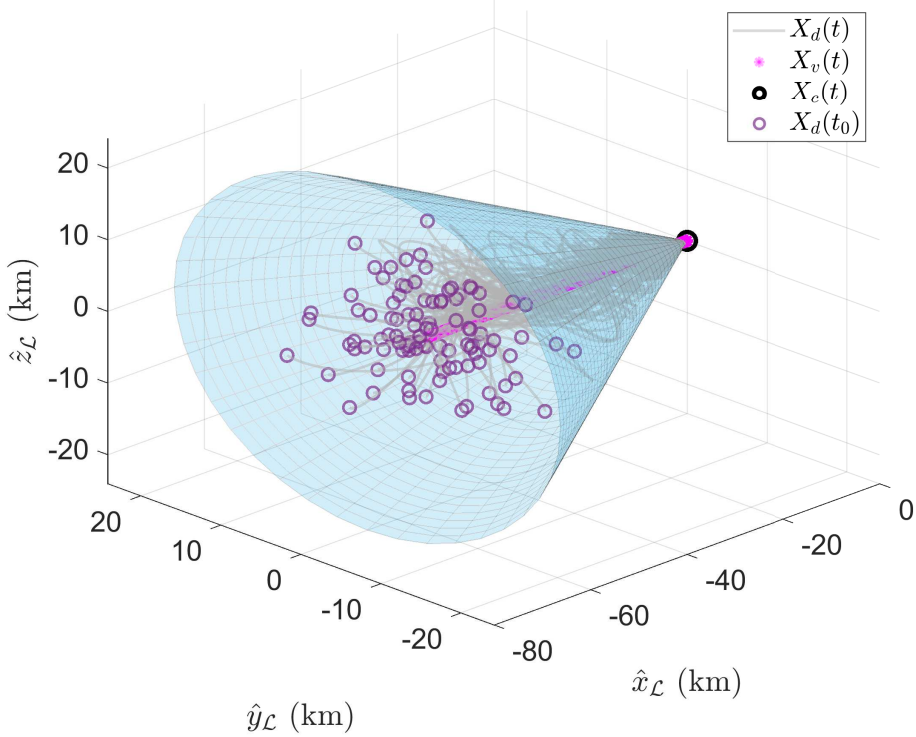


Fig. 5 Trajectories expressed in the VNB frame: the Deputy spacecraft’s path (gray line) tracks the virtual target’s trajectory (magenta asterisk).

100 different initial states of the Deputy spacecraft are tested.

Figure 5 illustrates the Deputy spacecraft trajectories in the VNB frame for 100 different initial conditions, marked as purple circles, using the L-TSG during RD missions. The L-TSG provides time-shifted Chief spacecraft trajectories, marked as magenta asterisks, to enforce various constraints for the Deputy spacecraft. For all simulations, the Deputy spacecraft with L-TSG is capable of completing the rendezvous with the Chief spacecraft, marked as a black circle, within the Line of Sight (LoS) cone, as shown in Fig. 5.

Figure 6 shows the mean of the relative position and velocity of the Deputy spacecraft with respect to the Chief spacecraft and the virtual target, respectively, for two orbit periods in the ECI frame. In Fig. 6a, the Deputy spacecraft starts 50 km away from the Chief spacecraft, behind the Chief spacecraft along the orbital track, and approaches the Chief spacecraft. During the one orbit period, the mean of the Deputy spacecraft trajectories reaches close to the trajectory of the Chief spacecraft in Figs. 6a, 6b. Then, the mean of the relative position and velocity of the Deputy spacecraft with respect to the Chief spacecraft maintains near zero after one orbit period, which means the Deputy spacecraft stays in the vicinity of the Chief spacecraft. Figures 6c and 6d provide the mean of the virtual target trajectories that are the closest target reference, along the reference orbital track, to the nominal closed-loop system to satisfy the constraints. Thus, the relative

| SMA, $a$          | Eccentricity, $e$ | Inclination, $i$ | RAAN, $\Omega$ | Argp, $\omega$ |
|-------------------|-------------------|------------------|----------------|----------------|
| 26646.680769 [km] | 0.74              | 1.096067 [rad]   | 0.0 [rad]      | 4.88692 [rad]  |

Table 2 Orbital elements of the reference Molniya orbit.

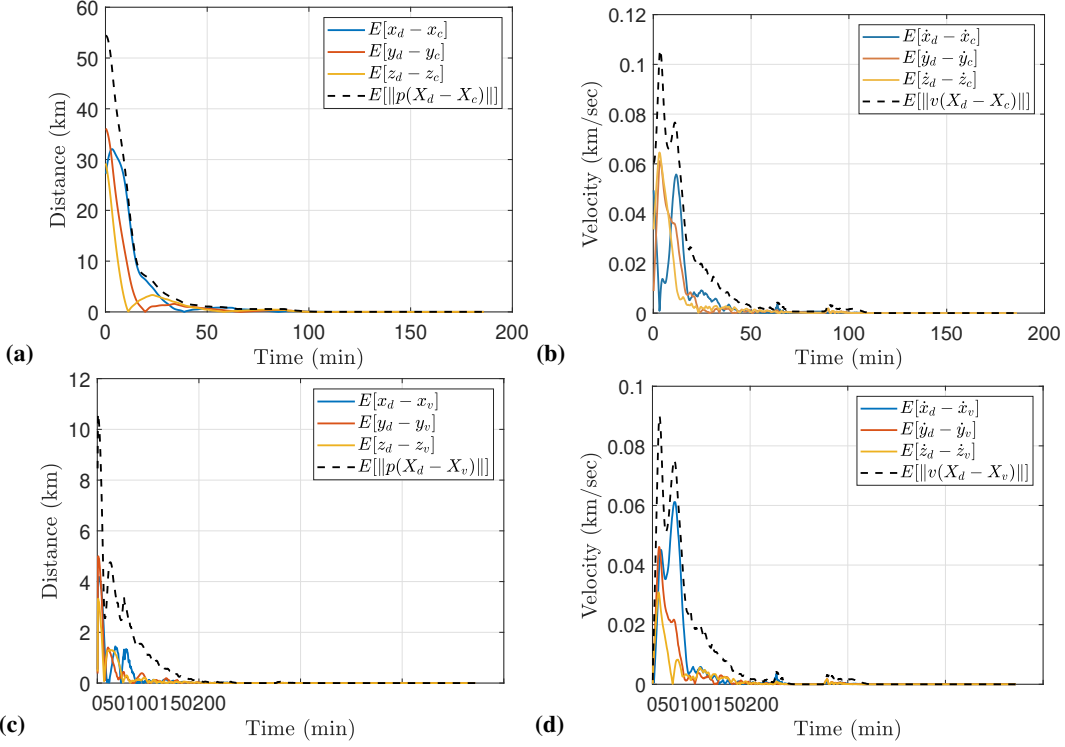


Fig. 6 Time histories of relative a) position; b) velocity to the Chief spacecraft; c) position; d) velocity to the virtual target.

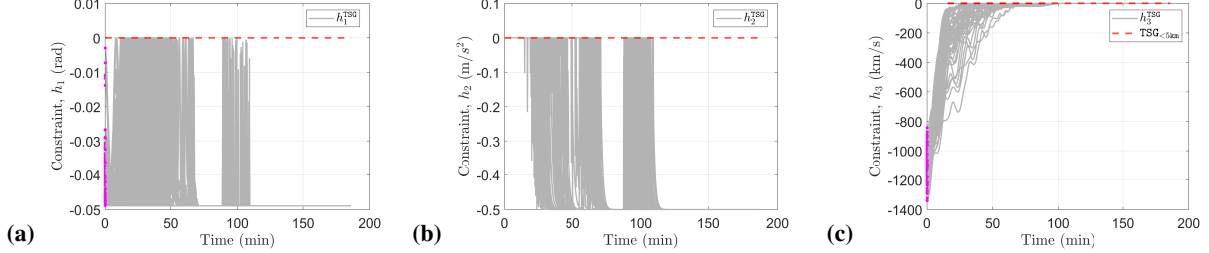


Fig. 7 Time histories of a) LoS cone angle constraint  $h_1$ ; b) thrust constraint  $h_2$ ; c) approach velocity constraint  $h_3$ .

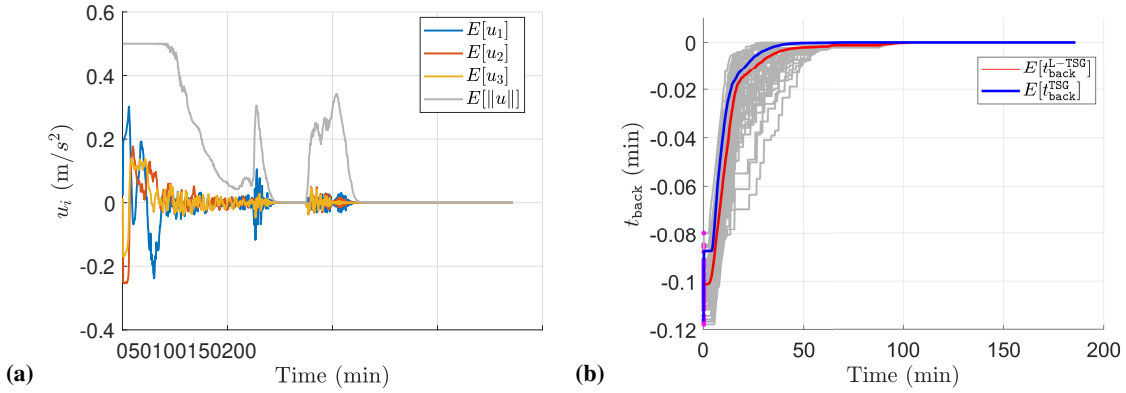


Fig. 8 a) Control input history and b) time shift history throughout the mission.

| $\delta x_0$ [km] | $\delta y_0$ [km] | $\delta z_0$ [km] | $\delta \dot{x}_0$ [km/s] | $\delta \dot{y}_0$ [km/s] | $\delta \dot{z}_0$ [km/s] |
|-------------------|-------------------|-------------------|---------------------------|---------------------------|---------------------------|
| -25.9809          | 27.8498           | 22.7715           | -0.0350                   | -0.0066                   | -0.0234                   |

Table 3 Expected initial state of the Deputy relative to the Chief, e.g.,  $\mathbb{E}[X_d(t_0) - X_c(t_0)]$ .

distance and velocity of the Deputy spacecraft with respect to the virtual target is smaller than that with respect to the Chief.

In Fig. 7, the time histories of three inequality constraints are presented from Monte Carlo simulations with perturbed initial conditions. Figure 7a provides the LoS constraint evolution during the RD mission, and the L-TSG is capable of enforcing the LoS cone angle constraint  $h_1$  for the perturbed initial conditions. Figure 7c shows the time histories of the relative velocity constraint  $h_3$  given varying initial relative velocities, and L-TSG is able to handle this constraint during the RD missions. Note that the thrust limit is applied by the saturation function in Eq. (9), instead of L-TSG, but it narrows the feasible set of the time shift by applying the limited thrust in the validation process. Monte Carlo simulation results show that the L-TSG effectively enforces these constraints, as the LSTM cell in the L-TSG captures complex patterns to estimate the optimal time shift parameter.

Figure 8b illustrates the trajectories of the time shift parameter  $t_{\text{back}}$  as a function of time in a Monte Carlo campaign. Starting with a valid initial time shift  $t_{\text{back}}(0)$ , the parameter gradually increases to zero using L-TSG. This indicates that the Deputy spacecraft follows the virtual target’s trajectory, without constraint violations, and eventually stabilizes near the Chief spacecraft. The deep learning model’s training process uses the MSE term to drive the time shift estimate toward the optimal solution, while the MSReLU term prevents estimates that would lead to constraint violations. As a result, L-TSG produces maximum admissible time shifts that guarantee safety, given the standard LQ controller as a nominal closed-loop system.

### C. Simulation in Molniya Orbit

We next apply L-TSG to a more challenging scenario: the Molniya orbit. The Molniya orbit is characterized by its high eccentricity, providing a different set of challenges for the control system compared to the nearly circular orbit of the Crew-3 mission.

In this scenario, the Chief spacecraft orbits along the highly elliptical Molniya orbit, while the Deputy spacecraft starts approximately 10 km behind the Chief. The initial conditions of the Deputy spacecraft relative to the Chief are summarized in Table 4. As in the Crew-3 mission, we conducted Monte Carlo simulations with 100 different initial states of the Deputy spacecraft to introduce variations and assess the robustness of the control system.

Figure 9 illustrates the Deputy spacecraft’s trajectories in the VNB frame for these 100 initial conditions. The L-TSG provides time-shifted Chief spacecraft trajectories (marked by magenta asterisks) to enforce various constraints on the Deputy spacecraft. In all cases, the Deputy spacecraft successfully completed the rendezvous with the Chief spacecraft (marked by a black circle) within the Line of Sight (LoS) cone, demonstrating L-TSG’s capability in handling the high-eccentricity orbit.

Figure 10 shows the mean relative position and velocity between the Deputy spacecraft and both the Chief spacecraft and the virtual target over two orbital periods in the ECI frame. In Fig. 10a, the Deputy

| $\delta x_0$ [km] | $\delta y_0$ [km] | $\delta z_0$ [km] | $\delta \dot{x}_0$ [km/s] | $\delta \dot{y}_0$ [km/s] | $\delta \dot{z}_0$ [km/s] |
|-------------------|-------------------|-------------------|---------------------------|---------------------------|---------------------------|
| -9.7168           | -0.3110           | 0.5869            | 0.0014                    | -0.0035                   | -0.0068                   |

Table 4 Expected initial state of the Deputy relative to the Chief, e.g.,  $\mathbb{E}[X_d(t_0) - X_c(t_0)]$ .

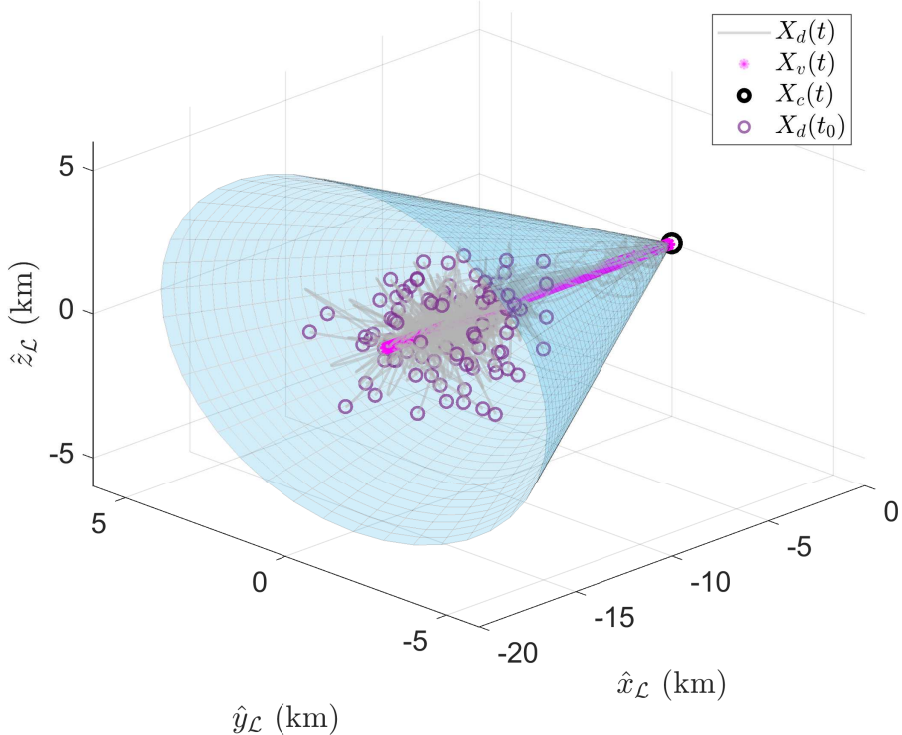


Fig. 9 Trajectories displayed in the local VNB frame: the deputy spacecraft’s path (blue line) closely follows the virtual target’s trajectory (magenta asterisk) in a highly eccentric orbit.

| Method | LEO           |                |                   | Molniya Orbit |                |                   |
|--------|---------------|----------------|-------------------|---------------|----------------|-------------------|
|        | Avg. Time (s) | Worst-case (s) | $\Delta V$ (km/s) | Avg. Time (s) | Worst-case (s) | $\Delta V$ (km/s) |
| TSG    | 0.1476        | 0.2057         | 1.2939            | 0.0852        | 0.1665         | 0.3558            |
| L-TSG  | 0.0233        | 0.0328         | 2.2477            | 0.0256        | 0.0323         | 0.9889            |

Table 5 Performance comparisons for spacecraft rendezvous missions

spacecraft starts 10 km behind the Chief and gradually approaches it. By the end of the orbital period, the Deputy spacecraft reaches and remains close to the Chief spacecraft’s trajectory (as seen in Figs. 10a and 10b). Similarly, the relative position and velocity with respect to the virtual target (Figs. 10c and 10d) show that the virtual target provides an effective reference for ensuring constraint satisfaction.

In Fig. 11, the time histories of the three main inequality constraints—LoS cone angle ( $h_1$ ), thrust ( $h_2$ ), and approach velocity ( $h_3$ )—are shown for the Monte Carlo simulations with perturbed initial conditions. Fig. 11a illustrates that L-TSG successfully enforced the LoS constraint throughout the simulation. Fig. 11c demonstrates that the relative velocity constraint was also effectively managed. Although the thrust constraint ( $h_2$ ) is enforced through saturation, the L-TSG manages the time shift to stay within the feasible set of constraints, as shown in Fig. 11b. These results indicate that the L-TSG handled this high-eccentricity, challenging orbit well. It dynamically adjusted the time shift in response to rapidly varying orbital conditions, ensuring that the Deputy spacecraft remained within safe operational limits.

The success of the L-TSG in this highly elliptic orbit can be attributed to several key factors. First,

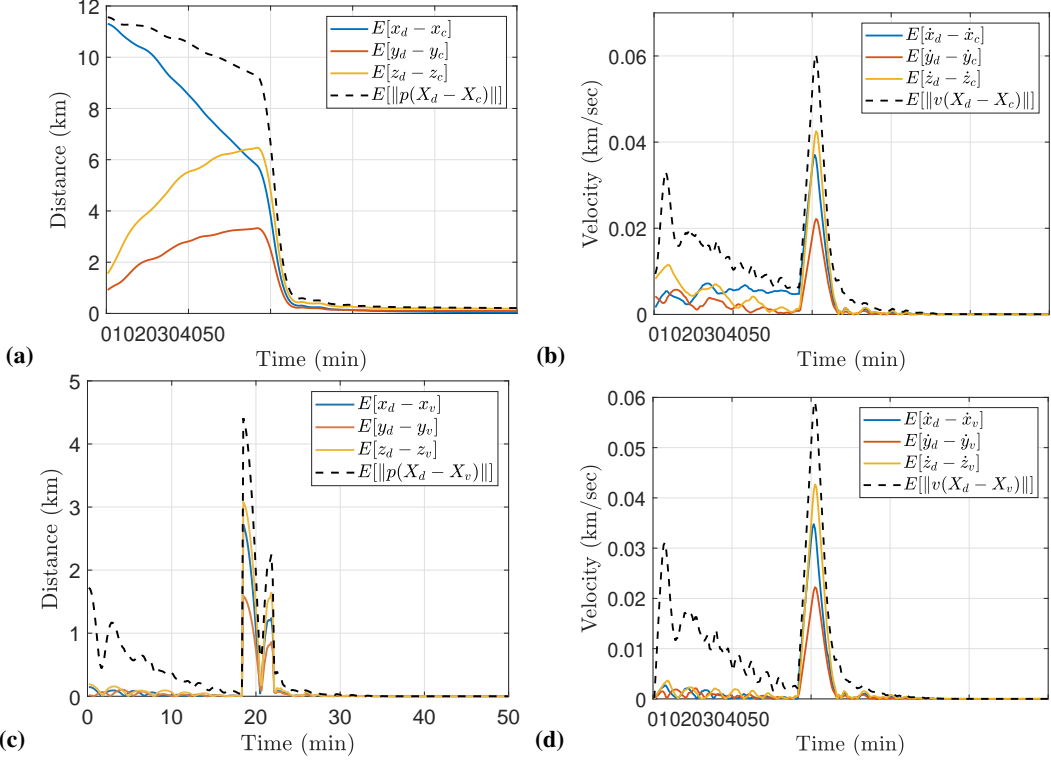


Fig. 10 Time histories of relative a) position; b) velocity to the Chief spacecraft; c) position; d) velocity to the virtual target, in an elliptical orbit.

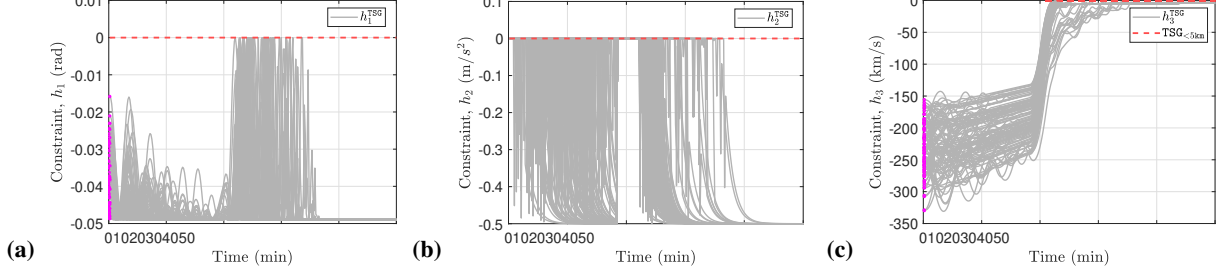


Fig. 11 Time histories of a) LoS cone angle constraint  $h_1$ ; b) thrust constraint  $h_2$ ; c) approach velocity constraint  $h_3$  for Monte Carlo simulations in a high-eccentricity orbit.

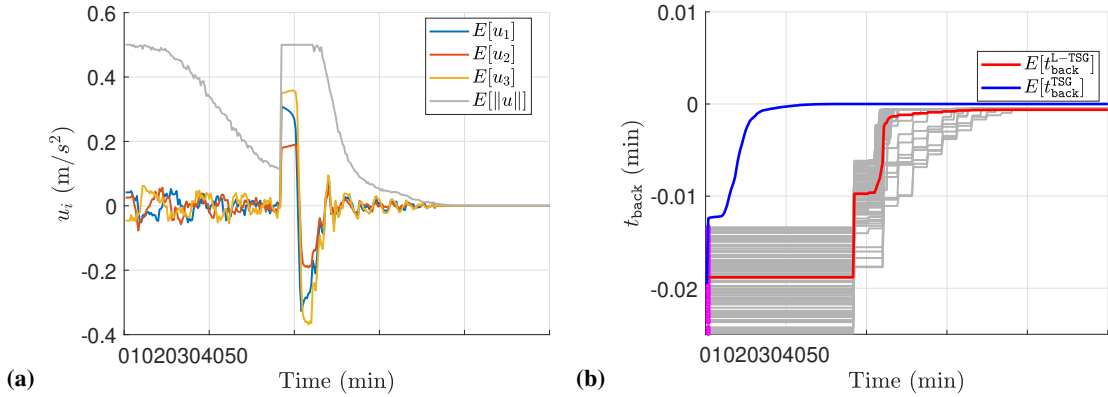


Fig. 12 a) Control input and b) time shift history throughout the mission in a Molniya orbit.

the high eccentricity of the Molniya orbit introduces significant variations in both velocity and distance during each orbital pass, which makes trajectory prediction and constraint enforcement more challenging. The LSTM-based deep learning model within L-TSG was able to capture the temporal dependencies and nonlinearities in these rapidly changing conditions, allowing for accurate time shift predictions. Additionally, the virtual target, calculated using the time shift, acted as a dynamic reference point that effectively guided the Deputy spacecraft to adjust its trajectory, even under these difficult conditions. This ensured that the spacecraft could maintain safe relative distances and velocities despite the large variations introduced by the orbit's eccentricity.

Finally, Fig. 12b displays the evolution of the time shift parameter  $t_{\text{back}}$  during the mission. The parameter starts at an initial value  $t_{\text{back}}(0)$  until the window size of 100 for the LSTM-based model is filled. Once the window is filled, the time shift gradually approaches zero as the Deputy spacecraft stabilizes near the Chief. This gradual adjustment is particularly significant in a highly elliptical orbit like Molniya's, where abrupt changes in velocity and distance are expected at different points along the orbit. The L-TSG efficiently handles these changes by incrementally updating the time shift, allowing the Deputy spacecraft to track the virtual target without constraint violations. The learning-based model, guided by the MSE and MSReLU terms, was able to predict time shifts that accounted for the eccentric orbit's challenging dynamics, avoiding solutions that would have led to constraint violations. This capability allowed the L-TSG to achieve a successful rendezvous with the Chief spacecraft despite the complexities of the orbit.

Compared to the conventional TSG, Table 5 shows that the L-TSG significantly reduces the onboard computation time for time shift parameter prediction. By using a prediction of the LSTM network, the L-TSG can generate the corresponding virtual target by checking the validity of the time shift, reducing computation times from 0.1476 s to 0.0233 s in LEO and from 0.0852 s to 0.0256 s in the Molniya orbit. When the Deputy spacecraft is far from the Chief spacecraft, the LSTM model updates a more accurate time shift than the prediction when it is near the Chief spacecraft. Depending on the relative distance, we replace an LSTM model, according to the PA-SW approach, to address this issue. Before the model transitions or mission completion, L-TSG potentially uses the backup plan of using the conventional TSG, but it can still contribute to computation time reduction for average and worst-case because of the narrowed bounds of the time shift set.

## VI. Conclusion

This study provides and demonstrates a novel framework that integrates a Time Shift Governor (TSG) with a learning-based model, called L-TSG, to accelerate the performance of TSG during rendezvous and docking (RD) missions in the Two-Body problem setting. By incorporating the learning-based model in our Monte Carlo campaign, L-TSG successfully avoided 95.4% of iterative processes in the bisection-based TSG during the Crew-3 mission and 95.1% during the Molniya orbit scenario. It showcases its capability to enforce state and control constraints during close rendezvous, including approach direction, relative velocity, and thrust limits. A target reference computed from L-TSG guides the closed-loop system to avoid constraint violations via a time-shifted state trajectory of the Chief spacecraft. The Deputy spacecraft conducts the RD mission until achieving the target reference, which aligns with the Chief spacecraft.

## References

- [1] Hartley, E. N., "A tutorial on model predictive control for spacecraft rendezvous," *2015 European Control Conference (ECC)*, IEEE, 2015, pp. 1355–1361.
- [2] Dong, H., Hu, Q., and Akella, M. R., "Safety control for spacecraft autonomous rendezvous and docking under motion constraints," *Journal of Guidance, Control, and Dynamics*, Vol. 40, No. 7, 2017, pp. 1680–1692.
- [3] Dong, H., Hu, Q., and Akella, M. R., "Dual-quaternion-based spacecraft autonomous rendezvous and docking

- under six-degree-of-freedom motion constraints,” *Journal of Guidance, Control, and Dynamics*, Vol. 41, No. 5, 2018, pp. 1150–1162.
- [4] Weiss, A., Baldwin, M., Erwin, R. S., and Kolmanovsky, I., “Model Predictive Control for Spacecraft Rendezvous and Docking: Strategies for Handling Constraints and Case Studies,” *IEEE Transactions on Control Systems Technology*, Vol. 23, No. 4, 2015, pp. 1638–1647. <https://doi.org/10.1109/TCST.2014.2379639>.
  - [5] Karr, C. L., and Freeman, L. M., “Genetic-algorithm-based fuzzy control of spacecraft autonomous rendezvous,” *Engineering Applications of Artificial Intelligence*, Vol. 10, No. 3, 1997, pp. 293–300.
  - [6] Huang, X., Li, S., Yang, B., Sun, P., Liu, X., and Liu, X., “Spacecraft guidance and control based on artificial intelligence: Review,” *Acta Aeronaut. Astronaut. Sin.*, Vol. 42, 2021, p. 524201.
  - [7] Wang, X., Wang, G., Chen, Y., and Xie, Y., “Autonomous rendezvous guidance via deep reinforcement learning,” *2020 Chinese Control And Decision Conference (CCDC)*, IEEE, 2020, pp. 1848–1853.
  - [8] Hovell, K., and Ulrich, S., “Deep reinforcement learning for spacecraft proximity operations guidance,” *Journal of spacecraft and rockets*, Vol. 58, No. 2, 2021, pp. 254–264.
  - [9] Federici, L., Benedikter, B., and Zavoli, A., “Deep learning techniques for autonomous spacecraft guidance during proximity operations,” *Journal of Spacecraft and Rockets*, Vol. 58, No. 6, 2021, pp. 1774–1785.
  - [10] Qu, Q., Liu, K., Wang, W., and Lü, J., “Spacecraft proximity maneuvering and rendezvous with collision avoidance based on reinforcement learning,” *IEEE Transactions on Aerospace and Electronic Systems*, Vol. 58, No. 6, 2022, pp. 5823–5834.
  - [11] Broida, J., and Linares, R., “Spacecraft rendezvous guidance in cluttered environments via reinforcement learning,” *29th AAS/AIAA Space Flight Mechanics Meeting*, American Astronautical Society, 2019, pp. 1–15.
  - [12] Xu, X., Zuo, L., and Huang, Z., “Reinforcement learning algorithms with function approximation: Recent advances and applications,” *Information sciences*, Vol. 261, 2014, pp. 1–31.
  - [13] Tipaldi, M., Iervolino, R., and Massenio, P. R., “Reinforcement learning in spacecraft control applications: Advances, prospects, and challenges,” *Annual Reviews in Control*, Vol. 54, 2022, pp. 1–23.
  - [14] Frey, G. R., Petersen, C. D., Leve, F. A., Garone, E., Kolmanovsky, I. V., and Girard, A. R., “Time shift governor for coordinated control of two spacecraft formations,” *IFAC-PapersOnLine*, Vol. 49, No. 18, 2016, pp. 296–301.
  - [15] Frey, G. R., Petersen, C. D., Leve, F. A., Garone, E., Kolmanovsky, I. V., and Girard, A. R., “Parameter governors for coordinated control of n-spacecraft formations,” *Journal of Guidance, Control, and Dynamics*, Vol. 40, No. 11, 2017, pp. 3020–3025.
  - [16] Kim, T., Liu, K., Kolmanovsky, I., and Girard, A., “Time shift governor for constraint satisfaction during low-thrust spacecraft rendezvous in near rectilinear halo orbits,” *2023 IEEE conference on control technology and applications (CCTA)*, IEEE, 2023, pp. 418–424.
  - [17] Kim, T., Kolmanovsky, I., and Girard, A., “Time Shift Governor for Spacecraft Proximity Operation in Elliptic Orbits,” *AIAA SCITECH 2024 Forum*, 2024, p. 2452.
  - [18] Han, Z., Zhao, J., Leung, H., Ma, K. F., and Wang, W., “A review of deep learning models for time series prediction,” *IEEE Sensors Journal*, Vol. 21, No. 6, 2019, pp. 7833–7848.
  - [19] Lara-Benítez, P., Carranza-García, M., and Riquelme, J. C., “An experimental review on deep learning architectures for time series forecasting,” *International journal of neural systems*, Vol. 31, No. 03, 2021, p. 2130001.
  - [20] Kolmanovsky, I. V., and Sun, J., “Parameter governors for discrete-time nonlinear systems with pointwise-in-time state and control constraints,” *Automatica*, Vol. 42, No. 5, 2006, pp. 841–848.

- [21] Ahmed, D. M., Hassan, M. M., Mstafa, R. J., et al., “A review on deep sequential models for forecasting time series data,” Applied Computational Intelligence and Soft Computing, Vol. 2022, 2022.
- [22] Yu, Y., Zhu, Y., Li, S., Wan, D., et al., “Time series outlier detection based on sliding window prediction,” Mathematical problems in Engineering, Vol. 2014, 2014.
- [23] Hota, H., Handa, R., and Shrivastava, A. K., “Time series data prediction using sliding window based RBF neural network,” International Journal of Computational Intelligence Research, Vol. 13, No. 5, 2017, pp. 1145–1156.
- [24] Heiney, A., “Top 10 Things to Know for NASA’s SpaceX Demo-2 Return,” <https://www.nasa.gov/humans-in-space/top-10-things-to-know-for-nasas-spacex-demo-2-return/>, July 2020. Retrieved 24 July 2020.
- [25] SpaceX, “Dragon,” <https://www.spacex.com/vehicles/dragon>, 2024. Accessed: 26 April 2024.